

Intrinsic and extrinsic corrugation of monolayer graphene deposited on SiO₂

V. Geringer¹, M. Liebmann¹, T. Echtermeyer², S. Runte¹, R. Rückamp¹, M. Lemme², and M. Morgenstern¹

¹*Institute of Physics,*

*RWTH Aachen University and JARA-FIT,
Otto-Blumenthal-Straße, 52074 Aachen*

²*Advanced Microelectronic Center Aachen (AMICA), AMO GmbH,
Otto-Blumenthal-Straße 25, 52074 Aachen*

(Dated: June 15, 2022)

Using scanning tunneling microscopy in ultra high vacuum and atomic force microscopy, we investigate the corrugation of graphene flakes deposited by exfoliation on a Si/SiO₂ (300 nm) surface. While the corrugation on SiO₂ is long-range with a correlation length of about 25 nm, the graphene monolayer exhibits an additional corrugation with a preferential wave length of about 15 nm. A detailed analysis shows that the long range corrugation of the substrate is also visible on graphene, but with a reduced amplitude, leading to the conclusion that the graphene is partly freely suspended between hills of the substrate. Thus, the intrinsic rippling observed previously on artificially suspended graphene exists as well, if graphene is deposited on SiO₂.

PACS numbers: 68.55.J-, 68.37.Ef, 68.37.Ps, 68.65.-k

Since it was believed, based on the Mermin-Wagner theorem, that two-dimensional (2D) crystals are not stable at finite temperature [1], it came as a surprise that monolayer graphene could be stabilized and identified on a Si/SiO₂ substrate [2, 3, 4]. Due to its peculiar properties like, e.g., a linear dispersion leading to Klein tunneling [5], high room-temperature mobility allowing quantum Hall steps without cooling [6], a low spin-orbit interaction beneficial for spintronic devices [7] or principally tunable spin-polarized edge states [8], graphene has meanwhile been intensively investigated. Already the first transport results revealing the absence of weak localization lead to the speculation of a curved surface [9], which acts as a phase-breaking field [10]. Such a curvature was indeed observed by microscopic electron diffraction of suspended monolayer graphene sheets [11]. The lateral wavelength of the isotropic curvature and the amplitude have been estimated to be $\lambda = 10 - 25$ nm and $A = 1$ nm, respectively. The behaviour has been reproduced theoretically by Monte-Carlo simulations with a preferential wavelength of 8 nm barely depending on temperature [12]. It is argued that the anharmonic coupling between bending and stretching modes in graphene triggered by the tendency to double-bond formation of carbon is responsible for the stability of the 2D crystal.

The corrugation properties of graphene on a SiO₂ substrate have been studied previously using scanning tunneling microscopy [13, 14] and non-contact atomic force microscopy [14]. Both studies reveal atomic resolution exhibiting hexagonal structures on the monolayer and triangular structures on the multilayer in agreement with expectations from symmetry. Long-range corrugations of subnanometer height and 20-40 nm length scale are found in both studies. They are attributed to the roughness of the underlying substrate. Here, we find the same long-range corrugations on the substrate as well as on the graphene, but, in addition, we find a more regular short wave-length corrugation with $\lambda \simeq 15$ nm and amplitude

of about 1 nm only on graphene. This is similar in wave length and amplitude to the corrugation observed on suspended graphene sheets [11]. Moreover, we find that the long-range corrugation has lower amplitude on graphene than on SiO₂ implying that the graphene is partly suspended between hills of the substrate, which might be favorable to develop the intrinsic short-scale rippling.

The graphene sample is fabricated by the mechanical exfoliation technique as described in [2, 15]. Using an optical microscope, a graphene flake containing a monolayer region is identified. Raman spectroscopy is used to confirm the number of layers with the help of the D2 line [16]. Fig. 1(a) shows three spectra measured in different areas of the flake visible in Fig. 1(b). In addition to a large monolayer area, we find smaller bi- and multilayer areas as marked by 1L, 2L and MuL, respectively. Next, gold contacts with a 10 nm Cr seed layer were deposited and structured with a lift-off process. Except for one side, the graphene sample is completely surrounded by the gold electrode as shown in Fig. 1(b). The mobility of graphene samples prepared identically but with several contacts exceeds $\mu = 1$ m²/(Vs) at 300 K [17]. In order to remove residual resist and adsorbates, the sample was rinsed in isopropanol and acetone, baked out to 150° C in air for four hours and, additionally, baked out to the same temperature in ultrahigh-vacuum (UHV) for three hours. The gold film served as the electrical contact for scanning tunneling microscopy (STM) and was used to prepare the STM tip (etched W) by voltage pulses. An instrumental challenge in UHV-STM investigations of microstructured samples is the accurate tip positioning. We used an optical long-distance microscope with a focal length of 30 cm and 5 μ m lateral resolution. Fig. 1(c) shows a microscopic image of the tip approaching the graphene flake in UHV. The home-built STM featuring an xy stage for lateral positioning and operating in UHV ($2 \cdot 10^{-7}$ Pa) is described in detail elsewhere [18, 19]. The xy stage has been checked to move accurately within 10

%. Topographic images are recorded applying the bias voltage V to the tip. Spectroscopic dI/dV curves are measured by lock-in technique using a modulation voltage V_{mod} . Therefore, we stabilize the tip at voltage V_{stab} and current I_{stab} before opening the feedback. STM images obtained at the intentionally irregular edge of the gold contact are displayed in the inset of Fig. 1 (b). They are used for orientation by STM and aid in finding monolayer, bilayer and multilayer areas on the flake.

Atomic force microscopy images are taken under ambient conditions in tapping mode using either a commercial cantilever with a silicon tip or an ultrasharp tungsten tip with a tip radius of 1 nm, which is attached at the bottom of a Si cantilever [20]. Imaging has been carried out in the attractive regime [21] with an oscillation frequency slightly above resonance.

Fig. 2 (b) and (c) show two atomically resolved STM images recorded on the monolayer (1L) and the multilayer (MuL) of graphene, respectively. One observes a hexagonal pattern on the monolayer and a triangular pattern on the multilayer in accordance with previous results [13]. The atomic resolution is still perceptible at lower resolution in Fig. 2 (a) and (d), but an additional irregular corrugation appears. Line sections shown in Fig. 2 (e) reveal that the corrugation height on this monolayer region is about 0.6 nm, a factor of three larger than on the multilayer region. A representative $dI/dV/(I/V)$ curve of the monolayer, which is known to represent the local density of states (LDOS) [22], is shown in Fig. 2 (f). As expected, it shows a V-like shape with the Dirac point close to 0 V. It does not change significantly across the area depicted in Fig. 2(d). Note that graphene on SiC(0001), in contrast, exhibits a much more complicated dI/dV spectrum [23, 24, 25]. The good representation of the graphene LDOS by $dI/dV/(I/V)$ and the continuous atomic resolution across Fig. 2d demonstrates the absence of resist on this part of the surface. Indeed, we found several large areas without resist, but still also areas where a remaining resist is apparent within the STM images. The fact that the Dirac point is observed close to 0 V shows a negligible influence of charging adsorbates, which are probably removed in UHV.

Fig. 3 (a) shows a large area STM image of the graphene monolayer. One observes a rather regular corrugation with amplitudes of more than 1 nm and a preferential distance between hills of about 15 nm. The histogram (not shown) is Gaussian with a full width at half maximum (FWHM) of 0.78 nm. The rms roughness is determined to be 0.36 nm. The latter two values fluctuate across the monolayer area by about 25 % (average rms roughness 0.32 nm), but the corrugation length scale remains constant. For comparison, Fig. 3(b) shows an AFM image of the bare SiO₂ surface recorded in tapping-mode. It is obvious that the corrugation on the substrate is lower and exhibits a larger length scale than the corrugation on graphene. The FWHM of the histogram of Fig. 3(b) is 0.48 nm and the rms roughness is 0.22 nm (average of all data (0.25 ± 0.05) nm). We used four dif-

ferent tips, including two ultrasharp tips with a tip radius of 1 nm [20], but always observed the same corrugation height and length scale, which, in addition, is in good agreement with previous results [14].

Careful inspection of the graphene monolayer in Fig. 3 (a) shows a modulation on top of the short-range corrugation exhibiting a similar length scale as the corrugation on the SiO₂ substrate. In order to disentangle the two contributions, we used two-dimensional autocorrelation functions of the two images [26], which are shown in Fig. 4 (a) and (b). Note that both figures use the same color scale, i. e. the intensities are directly comparable. A long-range structure represented by a central spot surrounded by four bright areas is visible in both images although with weaker intensity for graphene (a). Fig. 4 (c) shows the autocorrelation function of the graphene after removing the long-range part by high-pass filtering using a smooth (first order Butterworth) cutoff at wavelength $\lambda = 20$ nm. A preferential short-range distance is clearly visible by the strong spots around the center, but there is additional multiple correlation albeit not with high symmetry. Notice that creep and drift effects are carefully removed from the STM-images using the atomic resolution. Fig. 4 (d) shows radial line sections averaged over all angles of the correlation functions. The SiO₂ (black curve) exhibits a correlation length of about 25 nm comparable to [14] and, in addition, a very weak maximum at about 50 nm indicating a slight preferential distance between hills. The gray curve shows the radial line section of the high-pass filtered image of graphene visible in Fig. 4 (c). It exhibits a damped oscillation with a wavelength of about 14 nm looking very similar to correlation functions of liquids. For comparison, the radial line section of the autocorrelation function of the AFM image after applying the same high-pass filter is shown as a dotted line and does not exhibit any structure. We observe the damped oscillation also after high-pass filtering the original STM image in Fig. 3 (a) and determining the autocorrelation function afterwards. In addition, we checked that the obtained wave length is quite robust with respect to slight parameter changes of the filtering process. Depending on the filtering procedure and the selection of the minima or maxima used for determining the wave length, λ is varying by at maximum ± 2 nm with a mean value of $\lambda = 15$ nm.

From these results, we conclude that monolayer graphene can exhibit a rather regular short-scale corrugation not induced by the substrate. It is similar in height and wavelength to the one observed on suspended graphene [11] and calculated for freely suspended graphene by atomic Monte-Carlo methods [12]. This observation suggests that the graphene might be partly suspended even on the SiO₂ substrate. In order to verify this, we compared the Fourier components of the images of graphene and SiO₂ within the large wavelengths region $\lambda = 40 - 60$ nm (not shown). We indeed find that graphene exhibits a 50 % lower amplitude at all wavelengths within this wavelength range. This implies that

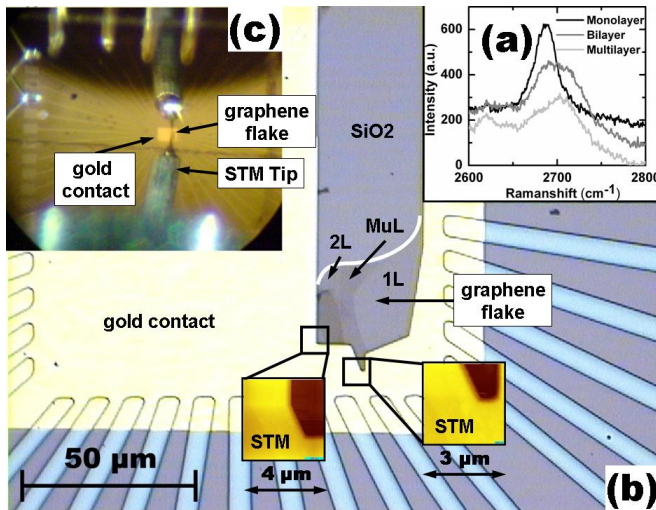


FIG. 1: (Color online) (a) Raman spectra using laser light of wavelength 532.1 nm. The spectra are recorded on different areas of the graphene flake and the attribution to monolayer, bilayer and multilayer is marked. (b) Optical image of the graphene sample with gold contacts. The different areas of monolayer (1L), bilayer (2L) and multilayer (MuL) as identified by Raman spectroscopy are indicated. Insets show two STM images acquired at the edge of the gold contact, which are used for orientation. (c) Microscopic image of the STM tip in tunneling contact with the graphene in UHV recorded with a long-range optical microscope.

the graphene does not follow the substrate corrugations exactly, but instead includes areas not in contact with the substrate. We believe that this partly free-standing configuration is the prerequisite for the intrinsic rippling of graphene. This might explain why the rippling was not found in previous STM investigations [13] and why weak localization is found in some samples [27] but absent in others [9], since the graphene/substrate contact will depend on details of the exfoliation process.

In summary, we have investigated graphene flakes on SiO_2 by UHV-STM and scanning tunneling spectroscopy. We identified monolayer and multilayer regions by Raman spectroscopy and their atomic appearance in STM images. A mesoscopic corrugation decreasing in amplitude with increasing thickness was found. This corrugation is not induced by the substrate and exhibits a preferential wavelength of about 15 nm and a rms roughness of 0.32 nm. Since the long-range corrugation of the substrate is additionally visible on graphene, but with smaller amplitude than on the substrate, we conclude that the rippled graphene is partly freely suspended.

We gratefully acknowledge useful discussions with G. Güntherodt, U. D. Schwarz and H. Kurz and financial support by FOR 912, project TP 6 of the Deutsche Forschungsgemeinschaft and by the German Federal Ministry of Education and Research (BMBF) under contract number NKNF 03X5508 ("ALEGRA").

- [1] N. D. Mermin, *Phys. Rev.* **176**, 250 (1968).
- [2] K. S. Novoselov, A. K. Geim, S. V. Morozov, D. Jiang, Y. Zhang, S. V. Dubonos, I. V. Grigorieva, and A. A. Firsov, *Science* **306**, 666 (2004).
- [3] Y. Zhang, J. W. Tan, H. L. Stormer, and P. Kim, *Nature* **438**, 201 (2005).
- [4] A. K. Geim and K. S. Novoselov, *Nature Mat.* **6**, 183 (2007).
- [5] M. I. Katsnelson, K. S. Novoselov, and A. K. Geim, *Nature Phys.* **2**, 620 (2006).
- [6] K. S. Novoselov, Z. Jiang, Y. Zhang, S. V. Morozov, H. L. Stormer, U. Zeitler, J. C. Maan, G. S. Boebinger, P. Kim, and A. K. Geim, *Science* **315**, 1379 (2007).
- [7] N. Tombros, C. Jozsa, M. Popinciuc, H. T. Jonkman, and B. J. van Wees, *Nature* **448**, 571 (2007).
- [8] Y. W. Son, M. L. Cohen, and S. G. Louie, *Nature* **444**, 347 (2006).
- [9] S. V. Morozov, K. S. Novoselov, M. I. Katsnelson, F. Schedin, L. A. Ponomarenko, D. Jiang, and A. K. Geim, *Phys. Rev. Lett.* **97**, 016801 (2006).
- [10] E. McCann, K. Kechedzhi, V. I. Fal'ko, H. Suzuura, T. Ando, and B. L. Altshuler, *Phys. Rev. Lett.* **97**, 146805 (2006).
- [11] J. C. Meyer, A. K. Geim, M. I. Katsnelson, K. S. Novoselov, T. J. Booth, and S. Roth, *Nature* **446**, 60 (2007).
- [12] A. Fasolino, J. H. Los, and M. I. Katsnelson, *Nature Mat.* **6**, 858 (2007).
- [13] E. Stolyarova, K. T. Rim, S. Ryu, J. Maultzsch, P. Kim, L. E. Brus, T. F. Heinz, M. S. Hybertsen, and G. W. Flynn, *Proc. Natl. Acad. Sci.* **104**, 9209 (2007).
- [14] M. Ishigami, J. H. Chen, W. G. Cullen, M. S. Fuhrer, and E. D. Williams, *Nano Lett.* **7**, 1643 (2007).
- [15] M. C. Lemme, T. J. Echtermeyer, M. Baus, and H. Kurz, *IEEE Elect. Dev. Lett.* **28**, 282 (2007).
- [16] A. C. Ferrari, J. C. Meyer, V. Scardaci, C. Casiraghi, M. Lazzeri, F. Mauri, S. Piscanec, D. Jiang, K. S. Novoselov, S. Roth, et al., *Phys. Rev. Lett.* **97**, 187401 (2006).
- [17] M. Lemme, T. Echtermeyer, M. Baus, B. Szafranek, J. Bolten, M. Schmidt, T. Wahlbrink, and H. Kurz, *Solid-State Electronics* **52**, 514 (2008).
- [18] J. Wiebe, A. Wachowiak, F. Meier, D. Haude, T. Foster, M. Morgenstern, and R. Wiesendanger, *Rev. Sci. Instrum.* **75**, 4871 (2004).
- [19] V. Geringer, S. Runte, M. Liebmann, and M. Morgenstern, to be published.
- [20] MikroMasch (www.spmtips.com), NSC15 (Si) and DP15/HiRes-W/AlBS (Si cantilever with W tip apex).
- [21] H. Hölscher and U. D. Schwarz, *Int. J. Non-Linear Mech.* **42**, 608 (2007).
- [22] J. A. Stroschio, R. M. Feenstra, and A. P. Fein, *Phys. Rev. Lett.* **57**, 2579 (1986).
- [23] V. W. Brar, Y. Zhang, Y. Yayon, T. Ohta, J. L. McChesney, A. Bostwick, E. Rotenberg, K. Horn, and M. F. Crommie, *Appl. Phys. Lett.* **91**, 122102 (2007).
- [24] G. M. Rutter, J. N. Crain, N. P. Guisinger, T. Li, P. N. First, and J. A. Stroschio, *Science* **317**, 219 (2007).

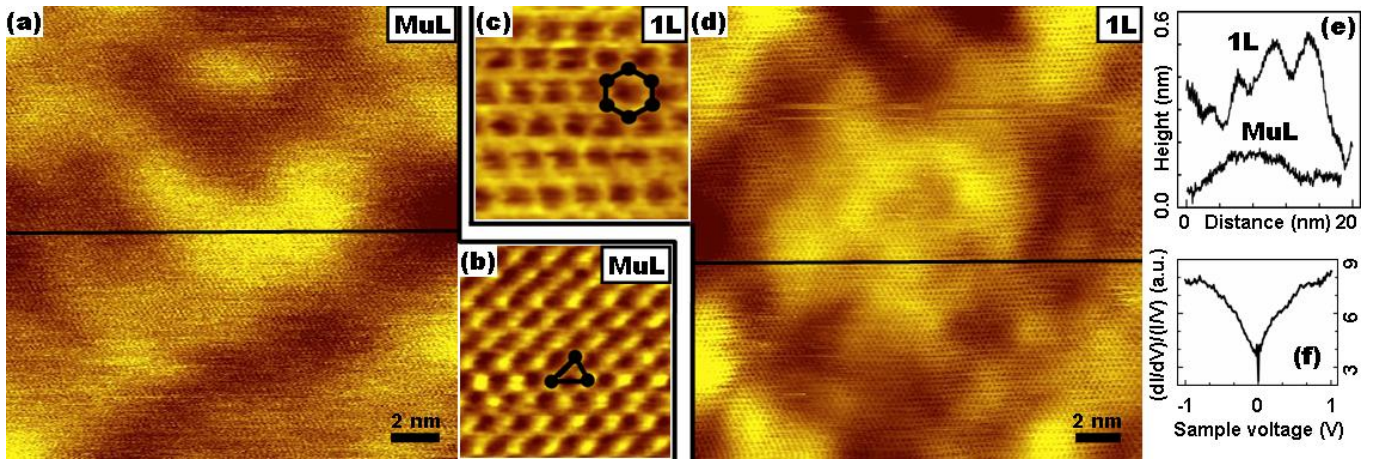


FIG. 2: (Color online) (a) Constant current STM image of multilayer graphene (0.4 V, 258 pA) (raw data). (b) Higher resolution STM image of the same area as in (a) (0.4 V, 198 pA). (c) High resolution STM image of graphene monolayer area (1 V, 394 pA). (d) Lower resolution STM image of monolayer graphene (0.5 V, 292 pA) (raw data). (e) Line section along the lines depicted in (a)(MuL) and (d)(1L). (f) Normalized dI/dV spectrum of monolayer graphene: $V_{\text{stab}}=0.7$ V, $I_{\text{stab}}=300$ pA, $V_{\text{mod}}=20$ mV.

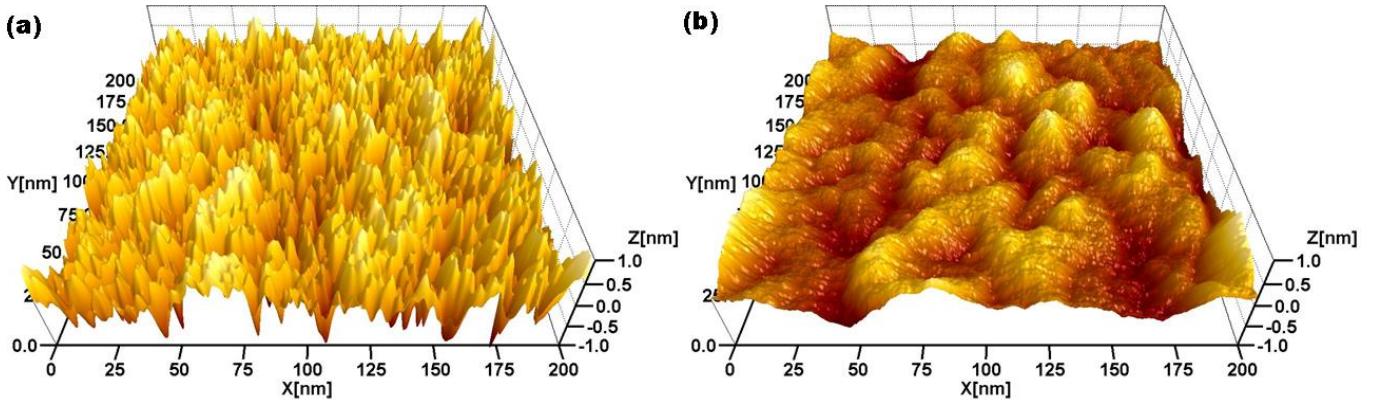


FIG. 3: (Color online) (a) 3D constant current STM image of monolayer graphene (1 V, 207 pA). (b) 3D tapping-mode AFM image of the SiO_2 substrate (resonance frequency 326.4 kHz, force constant 47 N/m, excitation frequency 326.5 kHz, oscillation amplitude 18 nm, constant amplitude feedback, setpoint 90%).

[25] P. Lauffer, K. V. Emtsev, R. Graupner, T. Seyller, L. Ley, S. A. Reshanov, and H. B. Weber, *Phys. Rev. B* **77**, 155426 (2008).

[26] I. Horcas, R. Fernández, J. M. Gómez-Rodríguez, J. Colchero, J. Gómez-Herrero, and A. M. Baro, *Rev.*

Sci. Instrum. **78**, 013705 (2007).

[27] F. V. Tikhonenko, D. W. Horsell, R. V. Gorbachev, and A. K. Savchenko, *Phys. Rev. Lett.* **100**, 056802 (2008).

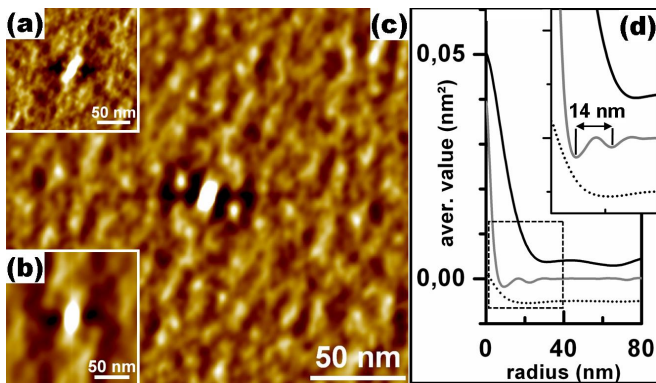


FIG. 4: (Color online) (a) 2D autocorrelation function of the drift corrected STM image of monolayer graphene as shown in Fig. 3(a). (b) 2D autocorrelation function of the AFM image of the SiO₂ surface as shown in Fig. 3(b), same color scale as in (a). (c) FFT high pass filtered image (1. order Butterworth, 20 nm) of the 2D autocorrelation function shown in (a). (d) Radial line sections of the unfiltered AFM autocorrelation image (b) (black), of the high pass filtered STM autocorrelation image (c) (gray), and of the high pass filtered AFM autocorrelation image (dotted). The inset shows a larger view of the area marked by the dashed line. The black and gray graphs are offset vertically for clarity.